Design and implementation of a bacterial signaling circuit

Lazova, M.D.

2013

document version
Publisher's PDF, also known as Version of record

Chapter 2

Response rescaling in bacterial chemotaxis

Sensory systems rescale their response sensitivity upon adaptation according to simple strategies that recur in processes as diverse as single-cell signaling, neural network responses, and whole-organism perception. Here, we study response rescaling in *Escherichia coli* chemotaxis, where adaptation dynamically tunes the cells' motile response during searches for nutrients. Using *in vivo* FRET measurements on immobilized cells, we demonstrate that the design of this prokaryotic signaling network follows the fold-change-detection (FCD) strategy – responding faithfully to the shape of the input profile irrespective of its absolute intensity – hitherto demonstrated only in eukaryotic cell sensory systems. Using a microfluidics-based assay for free swimming cells, we confirm intensity-independent gradient responses at the behavioral level. By theoretical analysis, we identify a set of sufficient conditions for FCD in *E. coli* chemotaxis, which lead to the prediction that the adaptation timescale is invariant with respect to the background input level. Additional FRET experiments confirm that the adaptation timescale is invariant over a ~10,000-fold range of background concentrations. These observations in a highly optimized bacterial system support the concept that FCD represents a robust sensing strategy for spatial searches.

This chapter has been published:

Lazova, M. D., Ahmed, T., Bellomo, D., Stocker. R., and Shimizu, T. S., Response rescaling in bacterial chemotaxis. *Proc Natl Acad Sci U S A* **108** (33), 13870 (2011).

Chapter 2

2.1. Introduction

Maximizing the information content of perceived signals is a non-trivial problem for biological systems, as it requires adaptive tuning of sensory responses to match the statistics of input signals [135]. Remarkably, strategies for inferring the likely distribution of inputs from recent experience appear to be 'hard coded' in many adaptive sensory systems, leading to well-defined relationships between the current response sensitivity and recent background inputs [247]. The most prevalent of such relationships is Weber's law, which prescribes that the magnitude of the immediate sensory response, Δr, following a small step change in input, Δs, is proportional to the ratio of the step size, Δs, to the background input level, s_0, *i.e.*, $\Delta r(\Delta s, s_0) = k\,\Delta s/s_0$, where k is a constant [81]. The underlying sensing strategy exploits a scenario commonplace in nature, where both the uninformative background intensity, s_0, and informative deviations from it, Δs, are proportionately scaled by a common source of signal power that fluctuates slowly in time – for example, sunlight which sets the brightness of images at different times of day [203]. Weber's law ensures that the response, Δr, remains invariant when both the stimulus, Δs, and the background, s_0, are rescaled by the same factor γ, *i.e.* $\Delta r(\Delta s, s_0) = \Delta r(\gamma\Delta s, \gamma s_0)$. This obviates the need to optimize the stimulus-response relation at every level of signal power.

Recently, a response rescaling strategy that applies to a broader class of input stimuli, called fold-change detection (FCD), has been described in a number of eukaryotic cell sensory systems [58,91,92]. FCD is conceptually similar to Weber's law – it yields invariant responses under proportionate scaling of the stimulus with the background – but it applies to the entire time series of the response, $\Delta r(t)$, to a stimulus time series, $\Delta s(t)$, not only to the instantaneous response following a step stimulus. In addition, FCD is not limited to small-amplitude stimuli, but applies also to time-varying stimuli of arbitrary amplitude and waveform. Thus, the FCD strategy prescribes scale-invariant responses to the complete input time series, $\Delta r(\Delta s(t), s_0, t) = \Delta r(\gamma\Delta s(t), \gamma s_0, t)$, and as such imposes more stringent design constraints on sensory systems than does Weber's law [231]. It has been hypothesized that FCD is a desirable property for sensory

systems guiding spatial searches by motile organisms [231], but whether and how any naturally occurring spatial guidance system implements the FCD strategy remains unknown.

Here, we study response rescaling in the signaling network of *E. coli* chemotaxis, which guides this bacterium's search for nutrients and is arguably the simplest sensory network known to exhibit adaptation over a broad dynamic range. Pioneering work by Adler and colleagues in the 1970's [171], as well as more recent work [115], has demonstrated logarithmic sensing behavior reminiscent of Weber's law in *E. coli*'s chemosensory system, which senses chemoeffector gradients as the bacterium samples its environment by swimming. Gradient sensing is achieved through temporal comparisons [218] mediated by fast and slow molecular processes [265]. On a rapid timescale, chemoeffector binding to transmembrane receptors produces an excitatory response, by modifying the activity of an intracellular signal that is relayed to the flagellar motor. On a slower timescale, enzyme-mediated covalent modification of the receptors restores pathway activity towards the pre-stimulus level, while also rescaling the sensitivity of receptors to ligand molecules [102].

The manner in which *E. coli* rescales its fast chemoreceptor response has been characterized in some detail by fluorescence resonance energy transfer (FRET) measurements of intracellular signaling. Using small-step stimulation by chemoeffectors, the response sensitivity was found to remain high at a nearly constant level over a broad range of background concentrations [241], confirming that Weber's law holds at the level of the rapid chemoreceptor response. Yet, biologically relevant inputs often vary slowly over time, because the high diffusivity ($D \sim 10^{-9}$ m^2/s) of small-molecule chemoeffectors leads to smooth concentration profiles in typical environments. To test whether *E. coli* demonstrates FCD in rescaling its chemotactic response to such smoothly varying inputs, we combine here FRET experiments encompassing both timescales of intracellular signaling with microfluidics-based assays of migration behavior. These experiments demonstrate that the dynamic output of the chemotaxis pathway activity is invariant under proportionate scaling of a time-varying stimulus with the background over a broad dynamic range. Thus, the *E. coli* chemotaxis system demonstrates FCD, as recently predicted on theoretical grounds [231].

By analyzing a theoretical model of *E. coli* chemotaxis [260], we find that FCD imposes more stringent constraints on the design of the signaling system than does Weber's law, and identify a set of sufficient conditions for FCD in terms of the molecular parameters of the system.

2.2. Weber's law and fold-change detection (FCD)

The output response of the chemotaxis system can be characterized by a single variable, $a(t)$, that corresponds to the activity of a central kinase, CheA, controlled by clustered chemoreceptors. CheA activity determines the concentration of the phosphorylated response regulator protein CheY, which in turn controls cell swimming behavior [265,266]. A FRET pair, consisting of CheY, and its phosphatase, CheZ, fused to yellow and cyan fluorescent proteins (YFP and CFP), respectively [242], provides a real-time readout proportional to $a(t)$ for timescales greater than the relaxation time of the CheY phosphorylation cycle. In addition to enabling studies on receptor sensitivity [76,240,241], this FRET system has been combined with time-varying stimuli to measure the *in vivo* kinetics of the adaptation enzymes CheR and CheB [226], which provide negative feedback through covalent receptor modification (reversible methylation at multiple sites) and determine the slower timescale of the adaptation response, τ_m.

To study how the temporal response of chemotactic signaling depends upon the background level, we conducted FRET experiments in which bacteria, adapted to a background concentration $[L]_0$ of the non-metabolizable attractant α-methyl-aspartate (MeAsp), were subjected to a time-varying stimulus $\Delta[L](t)$. The stimulus was applied by modulating the input in time, as $[L](t) = [L]_0 + \Delta[L](t)$, using a fluid mixing apparatus. Figure 2.1A shows results from an experiment in which the stimuli, $\Delta[L]_i(t)$, differed in amplitude but the inputs, $[L]_i(t)$, had otherwise identical waveforms, *i.e.* $[L]_i(t) \equiv [L]_{0,i}\lambda(t)$, where $[L]_{0,i}$ is the i-th background concentration. The dimensionless waveform $\lambda(t)$ was held constant between all stimuli in this experiment, so that the stimulus-to-background ratio, $\Delta[L]_i(t)/[L]_{0,i} = (\lambda(t) - 1)$, was invariant. For this scenario, we found that the response time series, $\Delta FRET(t)$, was very similar over a broad range of background concentrations ($[L]_0$ = 0.018–2.903 mM). In contrast, in

the experiment of Figure 2.1B the sequence of stimuli, $\Delta[L]_i(t)$, was the same as the last four stimuli in the experiment of Figure 2.1A but the background level was held constant at $[L]_0 = 0.229$ mM. In this case, the FRET response to each stimulus in the sequence differed in both amplitude and waveform. Thus, the response to time-varying stimuli is not determined by the absolute difference from the background, $[L](t) - [L]_0$, but rather by the fold change over the background, $[L](t)/[L]_0$, indicating that chemotactic signaling in *E. coli* exhibits FCD.

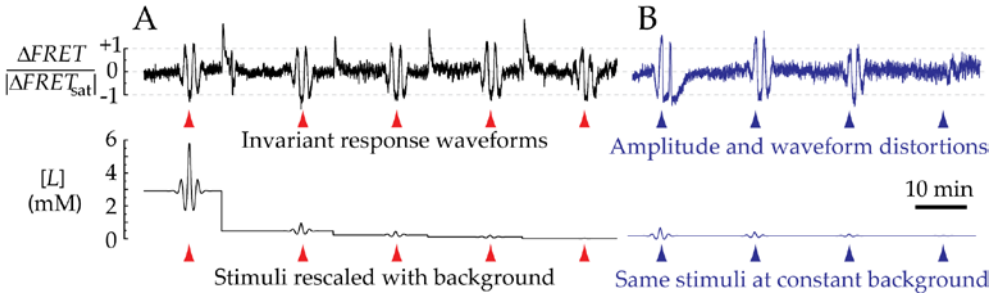

Figure 2.1. *E. coli* chemotaxis displays FCD. FRET response (top), $\Delta FRET$, normalized by the magnitude of the response to saturating stimuli ($|\Delta FRET_{sat}|$), of cells exposed to time-varying concentrations of MeAsp (bottom). **(A)** Response to five stimuli, $\Delta[L]_i(t)$, of identical waveforms and amplitudes scaled by the same factor as the background concentrations $[L]_{0,i}$ = (2.903, 0.478, 0.229, 0.109, 0.018) mM. **(B)** The last four stimuli, i = (2, 3, 4, 5) were repeated while the background was kept constant (0.229 mM). (The first stimulus, at $i = 1$, could not be applied at this background because $[L]_0 + \Delta[L]_1(t)$ would reach negative values at $[L]_{0,1} = 2.903$ mM.)

2.3. Dynamic range of FCD in *E. coli* chemotactic signaling

To probe the dynamic range over which FCD holds, we compared the temporal response profiles at different background concentrations in experiments of the type shown in Figure 2.1A. One can use any function for $\lambda(t)$ to test for FCD, which, by definition, holds for arbitrary input waveforms. We chose an oscillatory waveform with a frequency $\nu = 0.01$ Hz, close to the characteristic frequency of the system's adaptation kinetics, $\nu_m \approx 0.006$ Hz (at 22° C; [226]), with a Gaussian amplitude modulation to probe both the low-amplitude regime, where the stimulus-response relation is

expected to be linear (*i.e.*, $\Delta FRET \propto \Delta[L]$), and the high-amplitude regime, where the stimulus-response relation saturates (*i.e.*, $\Delta FRET \rightarrow \Delta FRET_{sat}$). Figure 2.2 shows the FRET response time series over a ~30,000 fold range of background concentrations. We identified four concentration regimes. For $[L]_0 < 0.018$ mM (Figure 2.2A), the response amplitude increased with the background concentration. We detected two adjacent but distinct regimes where FCD holds locally: at intermediate ($[L]_0 = 0.018$–0.229 mM; Figure 2.2B) and high ($[L]_0 = 0.815$–10.345 mM; Figure 2.2C) background concentrations, responses were invariant in both amplitude and waveform. We hereafter refer to these regimes as FCD1 and FCD2, respectively, and to the low concentration regime, where the response amplitude depended on the background level (Figure 2.2A), as "no FCD" regime. At very high concentrations (>10.345 mM; Figure 2.2D), osmotic stress perturbs the chemoreceptors [263] and this regime is not considered further.

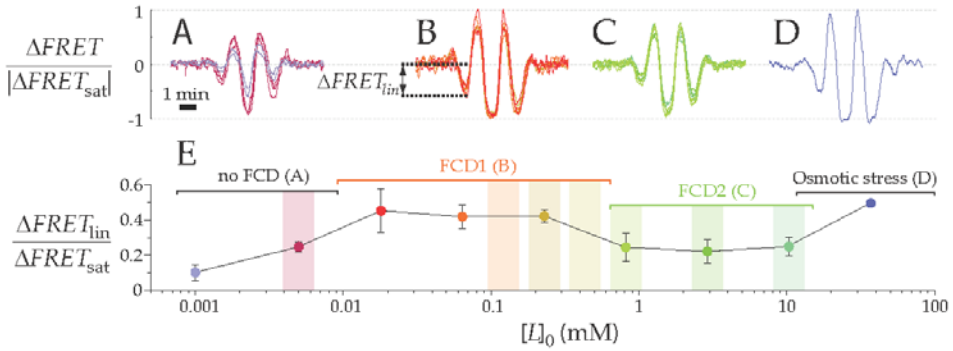

Figure 2.2. Dynamic range of FCD. (A-D) FRET response to a stimulus waveform (Figure 2.4B, blue curve) for different background concentrations $[L]_0$ = **(A)** 0.001 and 0.005 mM; **(B)** 0.018, 0.064 and 0.229 mM; **(C)** 0.815, 2.903 and 10.345 mM; **(D)** 36.871 mM. Two replicates for each concentration are shown. **(E)** Response amplitude, $\Delta FRET_{lin}$, for the same cases, computed as the peak in the linear response regime (see panel B). Vertical bars indicate the concentration ranges used in microfluidic gradient experiments (Figure 2.3).

The two FCD regimes differ in the response magnitude, most notably in the low-amplitude regime of the response, where $\Delta FRET \ll \Delta FRET_{sat}$ (Figure 2.2B, C). Therefore, we characterized the amplitude of the first negative peak, $\Delta FRET_{lin}$ (see Figure 2.2B), which was always much smaller than $\Delta FRET_{sat}$ and thus provides a good approximation of the response within the linear regime of the stimulus-response relation. $\Delta FRET_{lin}$ depends only weakly on background concentration (Figure 2.2E), with a <2-fold difference over a ~2000-fold concentration interval ($[L]_0$ = 0.005–10.345 mM). Interestingly, this dependence of amplitude on background concentration closely resembles the previously reported [241] step-response sensitivity of chemoreceptors (defined as $(\Delta a/a_0)/(\Delta [L]/[L]_0)$, where a_0 is the steady-state kinase output), suggesting that the dependence arises within the fast timescale chemoreceptor response.

2.4. FCD in population behavior of swimming *E. coli*

If the chemotactic signaling response is invariant under rescaling of temporal gradients by the same factor as the background level, a swimming *E. coli* cell might do equally well at climbing different spatial gradients when these are similarly rescaled. A single bacterium's trajectory is difficult to follow experimentally over extended times. However, the spatial distribution of an ensemble of cells is readily imaged over long periods. If FCD holds on the behavioral level, the spatial distribution of the population is predicted to evolve identically in different chemoeffector gradients, as long as bacteria are pre-adapted to concentrations scaled by the same factor as the fold-change in the gradients' magnitude.

To test this prediction, we studied the migration of swimming cells in spatial gradients of MeAsp, established in a microfluidic system (Figure 2.3A) of a type described before [7,52,115]. The device, consisting of polydimethylsiloxane (PDMS) and agarose, creates and maintains a steady linear MeAsp gradient. Bacteria are introduced into a W = 600 μm wide "test channel" patterned in the PDMS layer, which has one face open to the underlying agarose layer. A linear gradient is pre-established within the agarose by flowing buffer with different MeAsp concentrations in the two

flanking channels, higher in the "source channel" and lower in the "sink channel" (Figure 2.3A). A gradient mirroring that of the underlying agarose layer rapidly develops within the test channel, because of its small depth. We followed the migration of cell populations in the test channel by video-microscopy. Typical images of cell trajectories demonstrate that bacteria are initially uniformly distributed (Figure 2.3B, upper panel), but subsequently accumulate on the side closest to the source channel (Figure 2.3B, lower panel). Analysis of sequences of images yielded the bacterial distribution, $B(x)$, along the gradient.

We tested seven different gradients, each time rescaling the steepness of the gradient by the same factor as the mean concentration, $[L]_m$ (the shaded bars in Figure 2.2E). Figure 2.3C shows the temporal evolution of the spatial distributions of bacteria, $B(x)$. The left column corresponds to $[L]_m$ = 0.005 mM, within the "no FCD" regime. As expected from the low amplitude of the FRET response in this range (Figure 2.2E), the chemotactic accumulation was weak. For $[L]_m$ within each FCD regime (middle and right columns) the entire temporal evolution of $B(x)$ was invariant, despite the ~12-fold variation in $[L]_m$ among experiments. The accumulation was stronger within the FCD1 regime than within the FCD2 regime, consistent with the difference in sensitivity measured by FRET (Figure 2.2E).

The invariance of the distributions is demonstrated more quantitatively in Figure 2.3D, where we plot the time series of a dimensionless figure of merit, chemotactic migration coefficient (CMC) [156]. The latter is defined as $CMC(t) \equiv \frac{\langle x \rangle(t) - W/2}{W/2}$, where $\langle x \rangle(t) \equiv \int xB(x,t)dx$ is the population-averaged spatial coordinate of the bacteria, x (along the chemoeffector gradient), measuring the mean displacement of the population from the center of the channel. The $CMC(t)$ time series are nearly identical for gradients within each FCD regime (Figure 2.3D). Taken together with the FRET data, these results demonstrate that within each concentration regime where intracellular signaling responses are invariant, the chemotactic performance in spatial gradients is also invariant. Thus, the FCD property extends from intracellular signaling to the behavior of swimming cells.

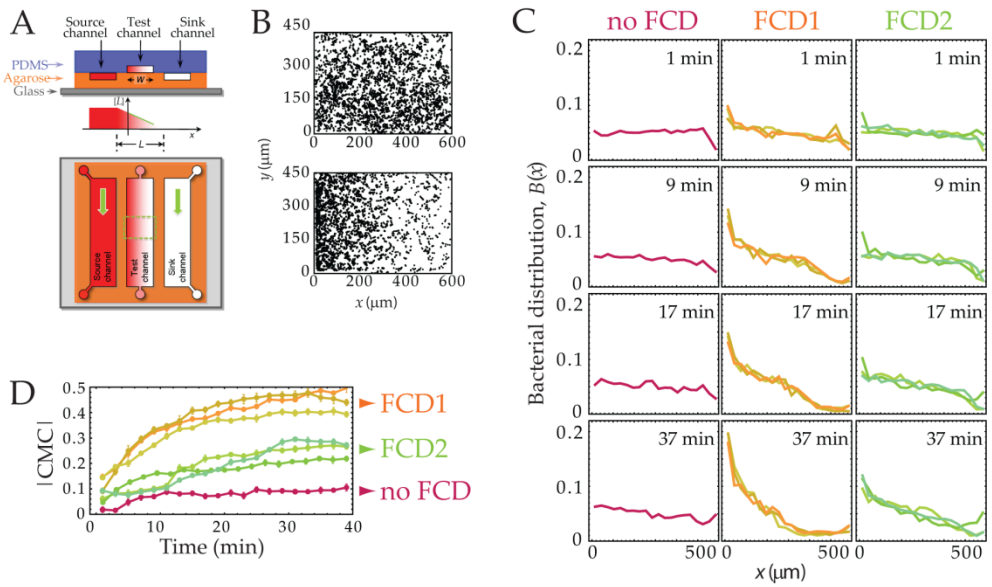

Figure 2.3. FCD demonstrated for swimming cells. **(A)** Schematic of the microfluidic device used to create a steady linear MeAsp gradient, of magnitude $\nabla[L]$ (see text). **(B)** Spatial distribution of chemotactic cells at the start of an experiment (top) and 19 minutes after establishment of a $\nabla[L]$ = 0.15 mM/mm gradient along $-x$ (bottom). **(C)** Time evolution of the bacterial distribution in gradients of differing magnitude, but identical fold-change. In each experiment, bacteria were pre-adapted to a concentration $[L]_m$ such that $\nabla[L]/[L]_m$ was constant (2/3 mm^{-1}). The values of $[L]_m$ (0.005, 0.120, 0.229, 0.430, 0.815, 2.903, and 10.345 mM) are also indicated in Figure 2.2E. **(D)** Time series of the absolute value of the chemotactic migration coefficient ($|CMC|$; see text).

2.5. Mechanistic requirements for Weber's law and FCD

To gain insight into the mechanistic requirements for FCD, we analyzed a coarse-grained model of the chemotaxis network that has successfully explained a large body of quantitative experiments on chemotactic signaling [260]. This model was shown to satisfy the general mathematical requirements for FCD, but those conditions alone do not fully constrain the possible molecular mechanisms [231]. Here we identify specific relationships between molecular parameters that lead to FCD-type response rescaling predicted to yield observable consequences. From a functional perspective, this model can be described as a negative feedback loop (Figure 2.4A) in which the ligand concentration, $[L](t)$, is the input, the

receptor-kinase activity, $a(t)$, is the output, and the average receptor methylation level, $m(t)$, is the feedback signal. The relationships between these variables are mediated by two transfer functions: $F(a)$, representing enzyme-driven methylation kinetics, and $G([L],m)$, representing cooperative kinase activation by chemoreceptors. The dependence of $G([L],m)$ on ligand concentration and methylation level is through a free energy difference, $f_t([L],m)$, between active and inactive states of the receptor-kinase complex, described by an allosteric two-state model of the Monod-Wyman-Changeux (MWC) type [176].

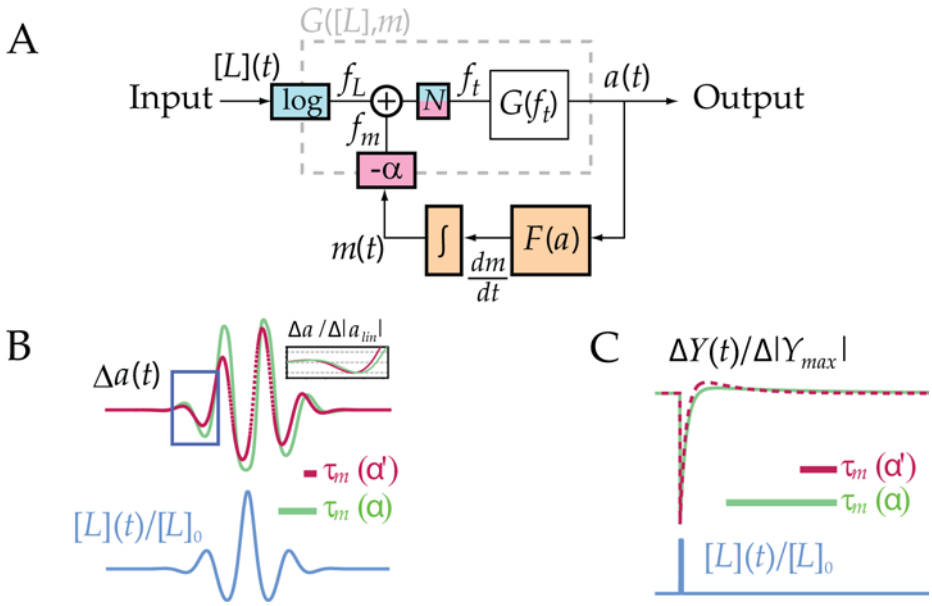

Figure 2.4. Requirements for FCD response rescaling. (A) Block diagram of the integral feedback network of *E. coli* chemotaxis. The receptor-kinase transfer function $G([L],m)$ constantly compares the ligand input $[L](t)$ with the methylation-feedback $m(t)$. Through another transfer function $F(a)$, the output $a(t)$ controls the rate of change of $m(t)$, yielding an integral-form feedback, which guarantees exact adaptation given appropriate conditions on $F(a)$. **(B-C)** Waveform distortions for sinusoidal (B) and impulse (C) stimuli, $[L](t)/[L]_0$ (blue curves), for a three-fold change in the response timescale, $\tau_m(\alpha)$, upon adaptation from one input level (green curves) to another (magenta curves). **(B: Inset)** Small-amplitude portion of the response (blue boxed region), with each response normalized by its amplitude. Note that the phase shift in the response in (B) and shape change in the impulse response in (C) are due to the difference in τ_m.

This model was previously used to explain Weber's-law-type response rescaling for step stimuli [260], which yielded a set of sufficient conditions on mechanistic parameters of this model. We find here that requiring FCD imposes an additional constraint on the design of the chemotaxis network, beyond those necessary for Weber's law, yielding the following as sufficient conditions for FCD:

I. Exact adaptation: the steady-state output, $a_0 = const$
II. Logarithmic coupling of ligand input, $[L]$, to the free energy, f_t: $\partial f_t / \partial \ln[L] = const$
III. Linear coupling of methylation feedback, m, to the free energy, f_t: $\partial f_t / \partial m = const$

All three of these constancy conditions must hold under changes in $[L]_0$. Exact adaptation (condition I; orange in Figure 2.4A) requires that the dynamics of the kinase activity, $a(t)$, has a unique globally stable fixed point. This is guaranteed by the integral feedback architecture of this pathway [286], provided that the transfer function, $F(a)$, is determined uniquely by the kinase activity, a, and crosses zero only once with a negative slope [260]. The remaining two conditions are constraints on the total free energy, which can be decomposed as $f_t([L], m) = N\big(f_L([L]) + f_m(m)\big)$, where $f_L([L])$ represents the contribution from ligand binding, $f_m(m)$ represents that from methylation, and N is the size of the cooperative receptor cluster. Logarithmic input coupling (condition II; blue in Figure 2.4A) means that the ligand effect on the total free energy, f_t, is proportional to the logarithm of ligand concentration. In MWC-type allosteric models, the assumption that both ligand-binding and the active $\leftrightarrow$ inactive transitions are thermally driven means that the ligand effect on activity depends on the distinct dissociation constants for the active and inactive states, K_A and K_I, through the relation $f_L([L]) = ln(1 + [L]/K_I) - ln(1 + [L]/K_A)$. Therefore condition II is satisfied for MWC models when the ligand concentration is in the range $K_I \ll [L] \ll K_A$ (where $f_L([L]) \sim \ln[L]$), given that the receptor cluster size, N, is also constant. Linear feedback coupling (condition III; pink in Figure 2.4A) signifies that the methylation effect on the total free energy, f_t, is directly proportional to the current methylation level, m.

Of these three conditions for FCD, conditions I and II are sufficient for Weber's law for step stimuli [260]. Thus, the only additional requirement for FCD is condition III, that the slope of the methylation-dependent free-energy must be a constant, i.e. $f_m(m)$ must be a linear function of m. Such a linear dependence was discovered in FRET experiments using step stimuli [226], where the function $f_m(m) = \alpha(m^* - m)$ yielded good fits to the data with $\alpha \approx 2$ and $m^* \approx 0.5$. The requirement for a constant α can be understood intuitively by examining the dynamics of this model, predicting that the characteristic timescale of adaptation, τ_m (defined as the relaxation time for the decay of the response, $\Delta a(t)$, after a small step change in the input) is inversely proportional to α: $\tau_m = \left(N a_0(1-a_0)\alpha F'(a_0)\right)^{-1}$. Thus, changes in α are expected to lead to distortions in the output waveform. In Figure 2.4B, C we illustrate the consequences of breaking this condition by numerical integration of a model that satisfies conditions I and II, but not condition III. For both smoothly varying stimuli (Figure 2.4B) and impulsive stimuli (Figure 2.4C), the response, $\Delta a(t)$, to the same input waveform, $\lambda(t)(= [L](t)/[L]_0)$, differs for two distinct feedback coupling coefficients α and α' (as could result from a nonlinear $f_m(m)$ when adapted to two different background concentrations). Thus, conditions I and II are not sufficient for FCD, even though this system will demonstrate response rescaling to step stimuli according to Weber's law.

2.6. Invariance of the chemotactic adaptation timescale

Our analysis of the requirements for FCD implies that the adaptation timescale, τ_m, is constant within each of the two FCD regimes identified in the FRET data (Figure 2.2). However, this observation does not rule out the possibility that τ_m depends on the background concentration over a broader range than each FCD regime. We reasoned that appreciable changes in τ_m would be observable as distortions in the output waveforms because this timescale directly determines the characteristic cutoff frequency, $\nu_m = (2\pi\tau_m)^{-1}$, for the linear signal filtering performed by the chemotaxis pathway [226,260]. Therefore, we compared the output waveforms between the two FCD regimes, as well as the "no FCD" regime, by superimposing the FRET response time series shown in Figure 2.2,

averaged within each of the three regimes (Figure 2.5A). The linear filtering analysis applies only for the small-amplitude regime of output, so inferring properties of τ_m from output waveform comparisons is only valid for the initial interval prior to saturation. When normalized by $|\Delta FRET_{lin}|$, responses within this interval (boxed region in Figure 2.5A) from all three regimes collapse onto a single output waveform (Figure 2.5A, *Inset*). Since large changes in τ_m would result in distortions of the output waveform, this collapse suggests the adaptation timescale, τ_m, is essentially invariant over the entire ~10,000-fold range of background concentrations spanned by these three regimes (Figure 2.4B inset).

To test more directly the invariance of τ_m, we subjected cells to exponential sinusoid inputs, $[L](t) = [L]_0 exp[A_L sin(2\pi\nu t)]$, perceived as pure sinusoids with amplitude A_L and frequency ν under logarithmic input coupling [226,260]. We recorded the response phase delay φ_D by fitting another sinusoid, $a(t) = a_0 + |A|cos(2\pi\nu t - \varphi_D)$, to the FRET response time series. At a fixed background concentration, the dependence of φ_D on ν was shown [226] to follow that expected for a linear filter, $\varphi_D(\nu) = \pi - tan^{-1}(\nu_m/\nu)$, so any dependence of $\tau_m = (2\pi\nu_m)^{-1}$ on $[L]_0$ can be detected as a change in φ_D upon stimulation at frequency ν. We measured this dependence at ν = 0.006 Hz (Figure 2.5B). The change in φ_D, if any, was very small (~0.02π per decade), corresponding to a <20% increase in τ_m over a >1,000-fold increase in $[L]_0$. Thus, both the time- and frequency-domain data strongly indicate that the adaptation timescale remains constant over a broad range of background concentrations[137].

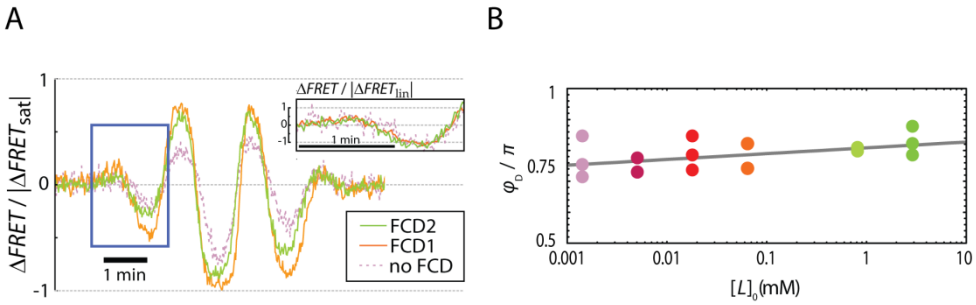

Figure 2.5. Invariance of the adaptation timescale over a ~10,000-fold range. (A) Overlaid view of output waveforms for the different background concentrations, separately averaged within the "FCD1", "FCD2" and "no FCD" regimes. The boxed region indicates the linear regime of the response. **(Inset)** The linear-regime response is invariant when rescaled by $|\Delta FRET_{lin}|$ (Figure 2.2B). **(B)** Phase delays, φ_D, for responses to exponential sinusoids with ν = 0.006 Hz and A_L = 0.2, for $[L]_0$ = 0.001, 0.005, 0.018, 0.064, 0.815 and 2.903 mM.

2.7. Discussion

We have shown that response rescaling in *E. coli* follows not only Weber's law at short times after stimulation, but also FCD over the entire response time series, in agreement with a recent theoretical prediction [231]. Unexpectedly, we identified two distinct FCD regimes which share a common adaptation timescale, but differ in their response amplitudes. As noted in a previous study of receptor sensitivity [241], a plausible explanation for these changes in the response amplitude for MeAsp is that more than one receptor species is involved in the response to MeAsp. Future experiments using mutant strains with altered receptor complements could shed light on this question (see Chapter 3).

The manner in which bacteria respond to temporal gradients is captured most succinctly by the system's response to impulsive stimuli (Figure 2.4C), whose characteristic biphasic shape demonstrates how inputs from different times in the past are weighed to produce the output at every instant. The particular shape of this time-dependent response function is expected to be under strong selection, as it determines how time derivatives are computed by the bacterium and, as such, encodes the basic

chemotactic strategy. The optimal response function for a given environment will depend on the typical distribution of nutrient sources and the shapes of the concentration fields they generate by diffusion. Much theoretical work has been devoted to the effects on chemotaxis of different response functions under a variety of environmental conditions [41,50,55,63,214], based on the impulse response obtained in classic experiments [36,218] that measured the response of flagellar rotation in cells tethered to a surface through their flagella. Our observation that the adaptation timescale is invariant with respect to the background level of input (Figure 2.5) validates the approach of using impulse response functions of the same shape to study gradient responses over the entire range of $[L]_0$ tested here, provided that the dependence of the amplitude of response on $[L]_0$ (Figure 2.2E) is taken into account.

How might FCD benefit a chemotactic bacterium? Shoval et al. [231] suggested that FCD could be advantageous in searching for nutrient sources. Their argument is based on the observation that typical environmental gradients generated by diffusion or convection from a source can have complex spatial profiles, but their characteristic shapes – when divided by the source strength – are invariant, *i.e.* the time-dependent spatial profile of the chemoeffector can be decomposed as $[L]([L]_0, \vec{x}, t) = [L]_0 \lambda(\vec{x}, t)$, where $[L]_0$ is the chemoeffector concentration at the source and $\lambda(\vec{x}, t)$ is a dimensionless profile that depends on the spatial coordinate, $\vec{x}$, and time, t, but not $[L]_0$. In this context, FCD enables a bacterium to focus on the shape of the profile as a signal encoding the source location, irrespective of the source strength. Such a strategy could be optimal when "any source is a good source", that is, the payoff for reaching even a weak nutrient source exceeds that for discriminating between the richness of nutrient sources. The search for nutrient patches by bacteria in the ocean, where microscale sources of dissolved organics are far between and highly variable in intensity [252], represents a tangible example of such a scenario. Comparatively little is known about the natural habitats of enteric bacteria such as *E. coli*, but the fact that this species, noted for its highly optimized physiology, demonstrates FCD invites further studies about phases in its life cycle and ecology that favor this robust search strategy.

Our results provide the first experimental demonstration of FCD in a sensory network guiding a spatial search, and of the consequences of FCD on organism- and population-level behavior. Given the arsenal of experimental and theoretical tools available for characterizing this minimal sensory network and its behavioral output, bacterial chemotaxis can serve as an ideal model system for further studies of FCD-type response rescaling, from the level of molecular mechanisms to its physiological and ecological implications.

2.8. Materials and methods

In vivo *FRET measurements and data analysis*

FRET microscopy of bacterial populations was performed [242]. The FRET donor–acceptor pair (CheZ-CFP and CheY-YFP) was expressed from a plasmid pVS88 [240] in a Δ(*cheY-cheZ*) *E. coli* RP437. Cells, attached to a poly-*L*-lysine-coated coverslip, were situated at the top face of a bespoke flow cell [27], and kept under constant flow (~ 2 ml/min) of motility buffer (10 mM potassium phosphate, 0.1 mM EDTA, 1 μM methionine, 10 mM lactic acid, pH 7), generated by a peristaltic pump (Rainin Dynamax RP1). Cells were subjected to time-varying input modulations, generated by mixing a concentrated solution of the chemoeffector α-methyl-*DL*-aspartate (MeAsp; Sigma Aldrich) and motility buffer by a fluid mixer of a type described before [35,226]. The output concentration [L](t) from the mixing chamber was controlled by modulating the in-flow rate, α, of the concentrated MeAsp using a computer-controlled syringe pump (Harvard Apparatus, PHD2000), whereas the in-flow rate of the motility buffer, β, was kept constant. Thus, $[L](t) = [L]^* \alpha(t)/[\alpha(t) + \beta]$, where $[L]^*$ is the MeAsp concentration in the syringe.

In the experiments shown on Figure 2.2 the background concentrations $[L]_0$ were equally spaced on a logarithmic scale by a factor $\gamma = (K_I K_A)^{1/4}$, centered about $[L]_{1/2} = (K_I K_A)^{1/2}$, where K_I and K_A are the dissociation constants for the inactive and active receptor states respectively. Cells, adapted to the i-th background, $[L]_{0,i} = \gamma^i [L]_{1/2}$, were subjected to an input $[L]_i(t) = \gamma^i S(t)$, where $S(t) = [L]_{1/2}\lambda(t)$, and in the

experiments of Figure 2.1, 2.2, and 2.5A, $\lambda(t) = exp\left(Ae^{-\delta^2(t-t_c)^2}\sin 2\pi\nu t\right)$, that is a sinusoidal waveform with frequency ν multiplied by a Gaussian pulse envelope with a peak of amplitude e^A at time t_c and a decay parameter δ. The frequency ν = 0.01 Hz was chosen to be close to the characteristic frequency, ν_m, of the system's adaptation kinetics [226]. Thus, changes in the adaptation kinetics would reveal themselves as phase shifts in the response. On the other hand, because receptor responses occur on much faster time scales, changes in receptor sensitivity would affect only the response amplitude, and not its waveform.

An upright microscope (Nikon FN1) was equipped with an oil immersion objective (Nikon CFI Plan Fluor, 40x/1.3). The sample was illuminated by a metal halide arc lamp with closed-loop feedback (EXFO X-Cite *exacte*) through an excitation bandpass filter (Semrock, FF01-438/24-25) and a dichroic mirror (Semrock, FF458-Di01). The epifluorescent emission was split by a second dichroic mirror (Semrock, FF509-FDi01) into donor (cyan, C) and acceptor (yellow, Y) channels and collected by two photon-counting photomultipliers (Hamamatsu H7422P-40) through bandpass filters (Semrock FF01-483/32 and FF01-542/27 for the C and Y channels, respectively). Detector output from the two channels were recorded through a data acquisition card (National Instruments) installed on a PC running custom-written software.

After background subtraction, the ratio between the acceptor and donor channel ($R = Y/C$) was used to compute the change in FRET efficiency upon stimulation: $\Delta FRET = \frac{R_{pre}+\Delta R-R_0}{R_{pre}+\Delta R+|\Delta Y/\Delta C|} - \frac{R_{pre}-R_0}{R_{pre}+|\Delta Y/\Delta C|}$, where where $\Delta R = R - R_{pre}$ is the ratio change, R_0 is the acceptor to donor ratio in absence of FRET, R_{pre} is the acceptor to donor ratio before stimulation, and $|\Delta Y/\Delta C|$ is the constant absolute ratio between the changes in the acceptor and donor signals per FRET pair ($|\Delta Y/\Delta C|\approx 0.6$) [242]. Under the conditions of the measurements $R_{pre} + |\Delta Y/\Delta C| \gg \Delta R$. Thus $\Delta FRET \sim \Delta R$, and we expressed $\Delta FRET$ for simplicity in arbitrary units of ΔR. $\Delta FRET(t)$ was normalized to the absolute magnitude of the response to saturating step stimuli $|\Delta FRET_{sat}|$, to compensate for variations due to different absolute signal levels between the experiments.

Microfluidic experiments and data analysis

Microfluidic chemotaxis experiments were performed in a hydrogel-based gradient generator (Figure 2.3A) [7], inspired by a design pioneered by Wu and colleagues [52]. A 1 mm thick agarose layer was sandwiched between a glass slide and a polydimethylsiloxane (PDMS; Sylgard 184, Dow Corning) layer. The microdevice consisted of three parallel channels, each 600 μm wide. Two 100 μm deep feeder channels ("source" and "sink" channels) were patterned in agarose and one 50 μm deep test channel in PDMS. The test channel was fabricated using standard soft lithography techniques [272]. The agarose layer was made from a 3% (w/v) solution of Ultra Pure Agarose (Invitrogen) in motility buffer, heated for 30 s in a 1250 W microwave oven and poured over a silicon wafer with positive reliefs of the feeder channels. After being allowed to gel at room temperature, the agarose layer was cut to size and used immediately or stored in motility buffer. Flexible polyethylene tubing (Cole-Parmer) and metal connectors (New England Small Tube Corp) were used to connect the inlets of the source and sink channels with two 0.5 ml glass syringes (Hamilton Company), driven by a syringe pump (PHD 2000, Harvard Apparatus), and the inlet of the test channel with a 1 ml plastic syringe (BD), operated manually.

A constant flow rate of 1 μl/min was maintained in the feeder channels, with two different concentrations of α-methyl DL aspartic acid (MeAsp; Sigma Aldrich) in the source and sink channel. Diffusion from the source to the sink, which are L = 1 mm apart (edge-to-edge), establishes a gradient across the agarose in ~20 min, and the concentration in the test channel reflects that in the underlying agarose. Because of the small height of the test channel, H = 50 μm, after introduction of the bacteria a gradient mirroring that of the underlying agarose rapidly develops in the test channel, within a time $H^2/2D < 10$ s (assuming a typical small-molecule diffusion coefficient for MeAsp, $D = 5\times10^{-10}$ m^2 s^{-1}). The gradient within the test channel was previously verified to be linear, with a magnitude equal to 69% of the gradient predicted assuming an exactly linear decay between source and sink channels [7]. The MeAsp concentrations in the source and

sink channels were varied between 0.005 and 10.345 mM, to generate gradients between 0.003 and 6.9 mM/mm.

After a suspension of *E. coli* RP437 ($OD_{600} \approx 0.5$) was manually injected in the test channel by suction, the inlet and outlet of the test channel were sealed with coverslips to prevent residual flow and evaporation. Chemotaxis experiments were conducted using a computer-controlled inverted microscope (TE2000-E, Nikon), equipped with a CCD camera (PCO 1600, Cooke). Bacteria were observed at test channel mid-depth, using phase contrast microscopy and a 20× objective. The subsequent chemotactic behavior of cell populations was followed by video microscopy [221]. Sequences of 200 frames sequence were captured at 10 frames per second every 2 min, from 1 to 39 min after injection of bacteria. Image analysis, using IPlab and MATLAB, was performed to determine bacterial positions in each frame. First, each frame was subtracted from the following one, to focus only on motile cells. Then motile bacteria were located in each frame as peaks in a monochrome intensity field. Bacterial positions were determined over all frames in a movie and binned to yield the the cell distribution $B(x)$ along the direction of the gradient.

FCD requires linear feedback coupling

In the model of Tu et al. [260], the dynamics of the chemotaxis pathway is captured by two equations:

$$\frac{dm}{dt} = F(a), \quad (1)$$

which describes the rate of change of the average receptor methylation level, m, as a function of the activity of the receptor-kinase complex, a, and

$$a = G([L], m) = G\big(f_t([L], m)\big) = \big(1 + e^{f_t([L],m)}\big)^{-1}, \quad (2)$$

which determines the receptor-kinase activity at every moment in time, given the current level of ligand input, $[L]$, and methylation feedback, m, via the free energy difference between the active and inactive states,

$$f_t([L], m) = N\big(f_L([L]) + f_m(m)\big), \quad (3)$$

where N is the number of ligand-binding receptor units cooperatively associated with each kinase molecule. If the free-energy contribution from

methylation feedback, $f_m(m)$, is removed, the remaining ligand-dependent part of this model for receptor kinase activity, equation (2), is formally equivalent to the Monod-Wyman-Changeux (MWC) model of allosteric proteins, widely used in biochemistry [176], and is also a limiting case of the Ising model of statistical physics [72,120,165]. As in the classical MWC model [176], the effect of ligand depends on the active and inactive states for the receptor having distinct affinities for ligand, leading to the expression

$$f_L([L]) = \ln \frac{1+[L]/K_I}{1+[L]/K_A}, \quad (4)$$

where K_I and K_A are the dissociation constants for the inactive and active receptor states, respectively. The methylation-dependent free energy, $f_m(m)$, is a feature that is not present in the classical MWC model, but has been shown experimentally to be well-approximated by a linear function,

$$f_m(m) = \alpha(m^* - m)\,, \quad (5)$$

where α is the slope of $f_m(m)$, and m^* is the offset methylation level at which $f_m(m) = 0$.

This model for *E. coli* chemotactic signaling is thus completely described by the MWC parameters N, K_I and K_A, which have been estimated in numerous studies utilizing data from FRET experiments with step stimuli [76,120,165,166,226,240,264], and the shapes of the functions $F(a)$ and $f_m(m)$, which were recently characterized by experiments with time-varying stimuli [226]. The picture that emerges from these studies is that both $f_L(\ln[L])$ and $f_m(m)$ are linear over a broad range. The linearity of $f_L(\ln[L])$ in the range $K_I << [L] << K_A$ follows from equation (4) with a large ratio between K_A and K_I values obtained in MWC-model fits to step-response data [166,226].

It has been shown previously [260] that for Weber's-law-type response rescaling for step stimuli, this model requires: I exact adaptation, satisfied by equation (1), and II a significantly extended linear regime of $f_L(\ln[L])$, which is achieved by the aforementioned large separation between the two dissociation constants: K_I = 0.018 mM, K_A = 2.903 mM for MeAsp binding to the aspartate receptor Tar [166,226]. Here, we demonstrate that FCD requires, in addition to I and II, a third condition, namely III that the methylation-dependent part of the receptor free energy, $f_m(m)$, is also linear.

Consider a system adapted to a background concentration $[L]_0$ at time t_0. Because the output time series $a(t)$ is determined solely by the free

energy, f_t, according to equation (2), demonstrating invariance in this free energy as a function of time, $f_t(t)$, under multiplication of the input $[L](t) = [L]_0 + \Delta[L](t)$ by a scalar constant γ suffices to prove FCD. Due to exact adaptation, the adapted state activity$a([L]_0, t_0) = a_0$, and hence also $f_t(t_0)$, is independent of the background level of input, $[L]_0$. On the other hand, solving equation (3) for the m makes clear that the adapted-state methylation level m_0 does depend on $[L]_0$,

$$m_0([L]_0) = f_m^{-1}\big(f_t(t_0)/N - f_L([L]_0)\big), \qquad (6)$$

where $f_m^{-1}(f)$ represents the inverse function of $f_m(m)$. Expressing the free-energy response time series as $\Delta f_t(t) = f_t(t) - f_t(t_0)$, we can write

$$\Delta f_t(t) = \Delta f_m\big(m(t)\big) + \Delta f_L\big([L](t)\big) \qquad (7)$$

where $\Delta f_m\big(m(t)\big) = f_m\big(m(t)\big) - f_m(m_0)$; $\Delta f_L\big([L](t)\big) = f_L\big([L](t)\big) - f_L([L]_0)$. Within the range $K_I \ll [L] \ll K_A$, $\Delta f_L\big([L](t)\big) = \Delta f_L\big(\gamma[L](t)\big)$, where γ is constant, because$f_L([L]) \sim \ln[L]$ in this range (equation 4). Requiring the time evolution of the total free energy, $\Delta f_t(t)$, to be invariant in equation (7) therefore requires the time evolution of $\Delta f_m(m(t))$ to also be invariant, *i.e.*,

$$\Delta f_m\big(m(t)\big) = f_m\big(m_0 + \Delta m(t)\big) - f_m(m_0) = \text{constant, at any time, } t, \qquad (8)$$

where $\Delta m(t) = \Delta m([L](t); t) \equiv m(t) - m_0([L]_0)$ is the time-dependent response to $[L](t)$ in the methylation level m. But if FCD holds, $\Delta m(t)$ is itself invariant under multiplication of the input by a factor γ, that is, $\Delta m(\gamma[L](t); t) = \Delta m([L](t); t)$, because it evolves according to the time integral of equation 1: $\Delta m([L](t); t) = \int_{t_0}^{t} F\big(a([L](t); t)\big)dt$, and $a(\gamma[L](t); t) = a([L](t); t)$ as required by FCD. On the other hand, m_0 depends explicitly on $[L]_0$ according to equation (6). Taking the derivative of equation (8) with respect to m_0, we see that FCD also requires

$$f_m'\big(m_0 + \Delta m([L](t); t)\big) - f_m'(m_0) = 0 \qquad (9)$$

For equation (9) to be true for an arbitrary input time series $[L](t)$, the local slope of $f_m(m)$ must be the same everywhere, that is, $f_m(m)$ must be a linear function.

Chapter 2

Alternative proof for the linear feedback coupling requirement

A more general and elegant proof of the linear $f_m(m)$ requirement for FCD has been communicated to us by Prof. Dr. Eduardo Sontag. This approach appeals to a general theorem for FCD developed in refs. [231] and [230], which, applied to the system of equations. (1) and (2), requires that, for FCD to hold, there must exist a function $R(p,m)$ that solves the following partial differential equation (a) with boundary condition (b):

(a) $\frac{\partial R}{\partial m}(p,m)F(a) = F(a)$ for all p, a, m;

(b) $G\big(p[L], R(p,m)\big) = G([L],m)$ for all p, a, m.

From (a) it follows that for all p, m, $\frac{\partial R}{\partial m}(p,m) = 1$, which gives $R(p,m) = m + r(p)$ for some function $r(p)$. This in turn implies from (b) that:

$f_L(p[L]) + f_m\big(m + r(p)\big) = f_L([L]) + f_m(m)$ for all $[L]$, m, p. (10)

Taking $\partial/\partial p$ in equation (10), we have

$[L]f_L'(p[L]) + r'(p)f_m'\big(m + r(p)\big) = 0$ for all $[L]$, m, p. (11)

And therefore, unless f_L is constant, there is at least some $p = p_0$ such that $r'(p_0) \neq 0$. (Because for some p_0 and $[L]_0$, $[L]_0 f_L'(p_0[L]_0) \neq 0$.) Now taking a derivative $\partial/\partial m$ in equation (11), we have $r'(p)f_m''\big(m + r(p)\big) = 0$ for all m, p, so that, in particular, $f_m''(m+q) = 0$ for all m, where $q = r(p_0)$. It follows that $f_m''(m) = 0$, so $f_m(m)$ is linear.

FCD implies an invariant adaptation timescale

Linearizing the equations (1) and (2) about the steady-state activity, a_0, we get

$\frac{d\Delta m}{dt} = F'(a_0)\Delta a,$ (12)

$\Delta a = \frac{\partial a}{\partial m}\Delta m + \frac{\partial a}{\partial [L]}\Delta[L],$ (13)

Adaptation kinetics can be characterized by the relaxation of activity after the application of a brief pulse of ligand, where the chemoeffector jump, $\Delta[L]$, has returned to zero (*i.e.* the relaxation of the

slow overshoot in Figure 2.4C). Differentiating equation (13) with respect to time, and substituting equation (12) yields

$$\frac{d\Delta a}{dt} = \frac{\partial a}{\partial m} F'(a_0)\Delta a = -\Delta a/\tau_m, \quad (14)$$

where we define

$$\tau_m \equiv -\left(F'(a_0)\frac{\partial a}{\partial m}\right)^{-1} = -\left(F'(a_0)\frac{\partial a}{\partial f_t}\frac{\partial f_t}{\partial f_m}\frac{\partial f_m}{\partial m}\right)^{-1} = \left(-\alpha N a_0(1-a_0)F'(a_0)\right)^{-1} \quad (15)$$

as the characteristic timescale of adaptation.

By inspecting this solution (equation 15), we can verify that the conditions for FCD imply an adaptation timescale that is insensitive to the background ligand concentration, $[L]_0$. Condition I (exact adaptation) ensures that the steady-state activity, a_0, and the methylation kinetics $F(a)$ are both invariant. Condition II (logarithmic input coupling) demands that $\frac{\partial f_t}{\partial \ln[L]} = N\frac{\partial f_L}{\partial \ln[L]}$ is constant, which means that N is constant within the range $K_I << [L] << K_A$, where $\frac{\partial f_L}{\partial \ln[L]}$ reduces to unity. Finally, condition III (linear feedback coupling) ensures that the remaining factor on the right hand side of equation (15), α, is also constant, confirming that τ_m is invariant under changes in $[L]_0$.

Waveform distortion due to changes in the adaptation timescale

We illustrated, through simple numerical simulations, the consequences of a violation of the invariance of the adaptive timescale τ_m (or equivalently of the feedback coupling coefficient α).

Figure 2.4B shows the time response to a sinusoidal waveform with Gaussian amplitude modulation (see Materials and methods). The responses depicted in Figure 2.4B were obtained by numerical integration of equations (1-3). The parameters were chosen as in [226]: N=6, a_0=1/3, m_0=0.5, K_I = 0.018 mM, K_A = 2.903 mM. The function $F(a)$ was described by a Michaelis-Menten equation with a variable gain

$$F(a) = V_R(1-a)/(K_R + 1 - a) - V_R(a)a/(K_B + a)$$
$$V_B(a) = V_B(0)\left(1 + \theta(a - a_B)\frac{a-a_B}{1-a_B}r_B\right) \quad (16)$$

where K_R and K_B are the Michaelis constants, and V_R and $V_B(a)$ are the maximal velocities of the methylation and demethylation reactions (catalyzed by CheR and CheB respectively). $V_B(a)$ is a piecewise linear function, the value of which remains $V_B(0)$ for values of a below a_B, and above a_B increases with a slope $r_B/(1-a_B)$ up to a maximal value $(1+r_B)V_B(0)$, implemented by use of a step function, defined as $\theta(x) = 1$ for $x > 0$, $\theta(x) = 0$ otherwise. The parameters in equations (16) are as reported in [226]: $V_R = 0.010\ s^{-1}$, $K_R = 0.32$, $K_B = 0.30$, $V_B(0) = 0.013\ s^{-1}$, $a_B = 0.74$, $r_B = 4.0$ The stimulus has a background concentration $[L]_0 = (K_I K_A)^{1/2} = 0.229$ mM and spans a time interval of 600s. The parameters of oscillatory waveform $\lambda(t)$ are $A = 0.69$, $\delta = 0.0112$, $\nu = 0.01$ Hz, $t_c = 325$. The feedback coupling coefficient α was set to 2 (magenta curve) and 6 (green curve).

Figure 2.4C shows the response time series for an impulsive stimulus. For an ideal impulse input, $[L](t) = \delta(t)$, where $\delta(t)$ is the Dirac delta function, such a response can be described as demonstrated in [260] by the function

$$\Delta Y(t \geq 0) = \Delta Y_0 \left[\frac{1}{\tau_m} e^{-\frac{t}{\tau_m}} - \frac{1}{\tau_z} e^{-\frac{t}{\tau_z}} \right]$$
$$\Delta Y(t < 0) = 0 \qquad (17)$$

where $\Delta Y_0 = -c_a k_a \frac{\tau_z \tau_m}{\tau_m - \tau_z} > 0$ and $c_a = -N a_0 (1 - a_0)$. The time constant τ_z represents the dephosphorylation time, and k_a is an effective phospho-transfer rate from CheA to CheY [260]. In Figure 2.4C, we choose $k_a = 10$, $N = 6$, $a_0 = 1/3$, $\tau_z = 10$s. The adaptation time scale τ_m was set to 3 s (magenta curve) and 9 s (green curve).

2.9. Acknowledgements

The microfluidics work was performed by Dr. Tanvir Ahmed in the group of Prof. Dr. Roman Stocker (Massachussetts Institute of Technology). Simulations were done by Dr. Domenico Bellomo (VU University, Amsterdam). Marco Seynen and Ilja Cerjak (AMOLF) contributed with FRET software development and instrument designs. Prof. Dr. Howard Berg brought the FCD topic to our attention.